

Purified high-sulfur coal as a fuel for direct carbon solid oxide fuel cells

Yong Jiao^{1,2}  | Xiaoting Xue¹ | Wenting An^{1,2}  | Paulo Sérgio Barros Julião² | Wei Wang² | Guangming Yang³ | Wei Zhou³ | Si-Dian Li¹

¹Institute of Molecular Science, Shanxi Key Laboratory of Materials for Energy Conversion and Storage, College of Chemistry & Chemical Engineering, Shanxi University, 92 Wucheng Road, Taiyuan 030006, China

²Department of Chemical Engineering, Curtin University, Perth, WA 6845, Australia

³Jiangsu National Synergetic Innovation Centre for Advanced Materials (SICAM), State Key Laboratory of Materials-Oriented Chemical Engineering, College of Chemical Engineering, Nanjing Tech University, 5 Xin Mofan Road, Nanjing 210009, China

Correspondence

Yong Jiao, Institute of Molecular Science, Shanxi University, 92 Wucheng Road, Taiyuan 030006, China; or Department of Chemical Engineering, Curtin University, Perth, WA 6845, Australia.
Email: jiaoyong@sxu.edu.cn; yong.jiao@curtin.edu.au

Funding information

Australian Research Council, Grant/Award Numbers: DP150104365 and DP160104835, DP160104835 and DP150104365; Natural Science Foundation of Shanxi Province, Grant/Award Number: 201601D102014; China Scholarship Council, Grant/Award Number: 201608140134; Shanxi Program for the Sci-tech Activities of Returnee Scholars, Grant/Award Number: 2014; Shanxi Coal-bed Methane Joint Foundation, Grant/Award Number: 2015012016; Shanxi Natural Science Foundation, Grant/Award Number: 201601D102014; Shanxi Key Technologies R&D Program, Grant/Award Number: 20150313003-3

Summary

The use of low-rank coal in a clean and efficient manner is a major challenge facing the current coal technology. A high-sulfur coal with 4.5 wt% sulfur is chosen to examine the compatibility of the pristine coal and the purified contrast with a solid oxide fuel cell (SOFC) with nickel cermet anodes. Desulfurization of the pristine coal is performed by molten caustic leaching method with a removal ratio of 80%. Analyses of the physicochemical properties of coal samples indicate that the purified coal has a more favorable structure and higher Boudouard reactivity, which is suitable as a fuel for fuel cells. The assessment of electrochemical performance reveals that the purification treatment not only makes the peak power density of SOFCs improve from 115 to 221 mW cm⁻² at 900°C but also extends their durability from 1.7 to 11.2 hours under a current density of 50 mA cm⁻² at 850°C with a fuel availability increasing from 6.25% to 40%. The postmortem analyses show that far less deposited carbon and nickel sulfide are observed on the anode surface. The fuel-based investigation reveals that the purified coal is a promising fuel for direct carbon fuel cells.

KEYWORDS

direct carbon fuel cell, durability, fuel compatibility, high-sulfur coal, molten caustic leaching purification, nickel cermet anode, solid oxide electrolyte, sulfur poisoning

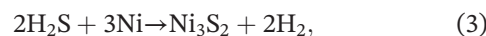
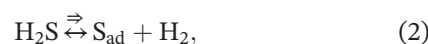
1 | INTRODUCTION

Coal is currently the second largest primary energy source after oil in the world, and it will remain a major energy source in the coming decades due to its extensive reserves in important energy economies.¹⁻³ Coal-fired power plants are the principal consumer of coal, which supply nearly 41% of the electricity globally and 70% to 80% of the electricity in China, India, and Australia.^{1,3} However, the major drawbacks of conventional coal-fired power generation are low conversion efficiencies (30%-40%) and a large quantity of CO₂ emissions (~2.7 kg of CO₂ per kg of coal).² Therefore, it is imperative to develop advanced coal power generation technologies with significantly higher conversion efficiencies and reduced environmental footprints.

Direct carbon fuel cells (DCFCs) are a promising electrochemical system that converts chemical energy of solid carbonaceous fuels into electricity with very high efficiency and concentrated CO₂ product streams that can be directly collected for industrial use or sequestration.⁴⁻⁷ Thermodynamically speaking, DCFCs offer 100% of conversion efficiency and up to 80% in practice, which nearly doubles the typical theoretical and real thermal conversion values found in thermal power plants, respectively.^{4,5} Compared with DCFCs with molten hydroxide or carbonate electrolytes, solid oxide electrolyte DCFCs (SO-DCFCs, or DC-SOFCs) offer many advantages in terms of high reliability and great fuel flexibility due to all solid-state construction and gasification-based fuel delivery mode.⁸⁻¹¹ In addition, a hybrid type of DCFC that combines a molten carbonate with a solid oxide electrolyte is under development to obtain a better performance.^{12,13} The feasibility of DC-SOFCs have been demonstrated by an integrated Boudouard gasification of solid carbon in the anode chamber.^{14,15} A series of studies have further illustrated the anode reaction mechanisms and the vital factors determining the performance of DC-SOFCs.¹⁶⁻¹⁹

Nickel-based cermets are the most commonly used anode materials for SOFCs owing to their superior performance in terms of activity towards hydrogen electrocatalytic oxidation, electronic conductivity, and thermo-mechanical compatibility with electrolytes.⁸ However, when using practical carbonaceous fuels, the nickel cermet anodes have to face many severe problems, such as sulfur poisoning and coke formation, which normally lead to rapid performance degradation.⁸ Coal is a complex heterogeneous conglomerate that usually contains a variety of organic and inorganic impurities. The compatibility problem between coal-derived solid carbonaceous fuels and the anode of DC-SOFCs is a major challenge for coal-based DC-SOFCs, because the anode materials such

as nickel cermets are quite vulnerable to the deleterious and deactivating effects of coal contaminants.^{1,4} Sulfur is the most notorious contaminant among the volatile coal contaminants such as S, P, Cl, As, and Sb in the form of their hydrides.²⁰ Even a H₂S content of 10 ppm can result in 90% nickel surface coverage at 1000 K.⁸ The cell voltage was stable below 4 ppm of H₂S spiked into a 50:50 CO-CO₂ fuel mixture at 850°C; however, it started to decrease quickly above 9 to 10 ppm of H₂S content.²¹ When the sulfur contents were higher than 20 ppm, sulfur poisoning may happen through an irreversible Ni oxidation and Ni₃S₂ formation route, which was primarily responsible for the performance deterioration.⁸ The mechanism of sulfur poisoning on nickel cermet anodes is briefly shown as follows:



where S_{ad} denotes the sulfur atoms adsorbed on the nickel surface. As shown in Equation 1, the reversible processes associated with the adsorption/desorption of sulfur are considered to be the predominant mechanism at relatively low sulfur concentrations. At a higher sulfur concentration, the preferable adsorption of sulfur on the nickel surface should occur (Equation 2). At the condition of the H₂S partial pressures greater than ~1%, an irreversible degradation of the anode would be observed, which can be associated with the formation of Ni₃S₂ (Equation 3). Although tremendous efforts have been devoted to improve the sulfur tolerance of nickel cermet anodes via various modification ways, the desulfurization for the coal fuel with high sulfur content still seems to be an essential method to prevent the anode from being exposed to most of the sulfur, ergo decreasing the amount of sulfur poisoning.^{1,3}

With the gradual depletion of high-quality coal reserves in the world, the efficient and clean usages of low-rank coal shift from important characteristics to mandatory properties in the current demands. Low-rank coal usually contains high ash, high sulfur and other trace elements. Among various purification methods of high-sulfur coal (HSC), molten caustic leaching (MCL) processes have a list of merits in terms of partial removal of the organic sulfur, and effective reduction of the contents of inorganic sulfur, minerals, and volatile matters of coal.²²

Recently, the feasibility of coal as fuel for DC-SOFCs has attracted more and more attentions.²³⁻³⁰ The peak

power density (PPD) of 89 mW cm^{-2} at 800°C was observed for the char of brown coal in DC-SOFCs.²⁴ An electrolyte supported SOFC using the lignite and lignite char as fuel reached the respective PPDs of 93 and 143 mW cm^{-2} both operating at 850°C .²⁶ Operating at the same temperature, a PPD of 100 mW cm^{-2} was achieved through a metallurgical coal char directly fed to a Ni-YSZ anode supported SOFC.²⁸ By impregnating the coal char with an Fe_mO_n -alkaline metal oxide catalyst and modifying its microstructure using alkali treatment, improved PPDs of 204 and 221 mW cm^{-2} were obtained again at 850°C , respectively.^{28,29} In fact, the impacts of mineral matter in coal on the performance of DC-SOFCs are diverse. Some of the metal oxides (like Fe_mO_n and CaO) in the mineral matter have catalytic effects on the Boudouard reaction, leading to an increase in CO content and a higher cell performance.^{24,28} On the other hand, the Si and Al ash compounds showed a negative effect on the durability by physically blocking the surface active sites and pore structures of anodes and suppressing the Boudouard reaction. An SOFC using ash-free coal prepared by thermal extraction achieved a power density of 170 mW cm^{-2} at 900°C , which provides a distinctly more durable operation than that of raw coal.²⁵ After a nitric acid demineralization of coal fuels, the PPD of an SOFC was improved from 90 to 120 mW cm^{-2} at 850°C .²⁷

Up to now, however, it is rare to find information in literature about the compatibility of purified HSC (PHSC) with the nickel cermet anode SOFCs. Herein, the coal samples with 4.5 wt% of total sulfur are chosen as a model of HSC, and the MCL process is adopted for purification. The compatibility of the pristine and purified coal samples with the nickel cermet anode SOFCs is examined. Based on characterizing the physicochemical properties of coal samples, the electrochemical performances are measured and analyzed in detail.

2 | EXPERIMENTAL

2.1 | Preparation of coal samples

The HSC was obtained from Shanxi Jincheng Anthracite Mining Group Co, Ltd (JAMG), China. The raw HSC was ground by agate mortar and sieved to 75 to $100 \mu\text{m}$ particle sizes. The purification of HSC samples was conducted by MCL method to remove sulfur, mineral matter, and other impurities in it.²² The HSC sample of 5 g was mixed with sodium hydroxide in the weight ratio of 1:2. The mixture was heated to 390°C at a rate of $10^\circ\text{C min}^{-1}$ in a muffle furnace and then held at 390°C for 2 hours. After cooling down to room temperature, the solid product was washed repeatedly with distilled water and then with 10% of HCl solution and distilled water until a nearly

neutral pH was reached. Finally, the PHSC sample was dried in an oven at 110°C for 2 hours.

2.2 | Characterization of coal samples

Proximate and ultimate analyses of HSC and PHSC samples were performed using an automatic industrial analyzer (5E-MAG6600B, Kaiyuan, China) and an elemental analyzer (Vario M-CUBE, elemental, Germany), respectively. X-ray diffractometer (XRD; D8 Advance, Bruker, Germany) was used to investigate the phase compositions and crystallinity of HSC and PHSC samples. The sample was packed into the circular cavity of a vitreous sample holder and scanned in a step-scan mode (0.02° per step) over a 2θ range from 10° to 80° (40 kV, 200 mA, Cu K α radiation). The crystalline structure parameters of the sample were estimated by the (002) and (100) diffraction peaks according²⁸ to Equations 4 and 5:

$$d_{002} = \frac{\lambda}{2 \sin(\theta_{002})}, \quad (4)$$

$$L = \frac{K\lambda}{\beta \cos\theta}, \quad (5)$$

where λ is the X-ray wavelength (0.15418 nm), θ_{002} is the diffraction angle of the (002) peak, d_{002} is the (002) crystal-line interplanar spacing, K is the shape factor, and β is the peak width at the half maximum intensity of the (002) or (100) peak. The crystallite size perpendicular to the basal plane, L_c , is calculated from the obtained (002) reflection, and the crystallite size parallel to the basal plane, L_a , is calculated using the (100) reflection. K values of 0.89 and 1.84 are used to calculate L_c and L_a , respectively.²⁹

As a method complementary to XRD diffraction analysis, the Fourier transform infrared spectroscopy (FTIR; Tensor 27, Bruker, Germany) was applied to identify the organic and inorganic impurities in the sample with 4 cm^{-1} of resolution between 4000 and 400 cm^{-1} . Before the FTIR measurement, samples were dried at 105°C overnight. Then the dried sample was mixed with KBr at the weight ratio of 1:100 evenly by grinding in agate motor, then pressed into transparent sheets for test. Nitrogen adsorption experiments were conducted using an automated surface area and pore size distribution analyzer (ASAP-2020M, Micromeritics, US). Prior to adsorption measurements, samples were degassed at 200°C for 24 hours under vacuum. N_2 adsorption isotherms were measured at 77 K over a relative pressure (P/P_0) range from 0.01 to 0.99. The specific surface areas of samples were calculated using the multiple-point Brunauer-Emmett-Teller (BET) method. The thermal stability and

oxidation reactivity of samples were conducted using a thermogravimetric analyzer (Evolution 16/18, Setaram Instrumentation, France) under Ar and air (21.2% O₂, balance N₂) at a flow rate of 80 mL min⁻¹. The sample of 10 mg was ramped up to a rate of 10°C min⁻¹ in an aluminum crucible, and the thermal effects within a temperature range of 25 to 1000°C were measured by thermogravimetric (TG) and differential thermogravimetric (DTG) methods.

2.3 | Fuel cell fabrication and testing

The anode-supported solid oxide fuel cell (SOFC) was used in this study, with NiO-yttrium stabilized zirconia (YSZ; Tosoh) (NiO:YSZ = 60:40, wt%) anode, YSZ electrolyte and La_{0.8}Sr_{0.2}MnO₃ (LSM) cathode, fabricated using a modified procedure from the literature.³¹ The electrolyte and anode layers were co-sintered in air at 1400°C for 5 hours to densify the electrolyte layer. The active cathode area of the SOFC single cell was 0.48 cm². The SOFC test setup is shown schematically in Figure 1. For the test, the single cell was sealed onto a thick quartz tube using silver paste with the cathode exposed to ambient air. The coal sample was placed near the anode surface using asbestos as support. Another thin quartz tube was positioned below the solid fuel layer to allow gases to be fed into the anode side and the reaction products to be released. Current-voltage curves were obtained using a 4-terminal configuration to eliminate the ohmic loss in the silver wires. Electrochemical impedance spectra (EIS) data were

collected with an Iviumstat electrochemical analyzer (Ivium Technologies B.V, Netherlands) under a frequency range from 0.1 Hz to 1 MHz using an alternate current signal amplitude of 10 mV. The availability tests for the samples of 160 mg (of HSC) and 150 mg (of PHSC) were performed at a constant current density of 50 mA cm⁻² under 850°C. A scanning electron microscope (SEM; JEM-2100, JEOL) coupled with an embedded energy dispersive X-ray analyzer (EDX) was used to determine the impurity elemental content of Ni-YSZ anode after the stability test of cells.

3 | RESULTS AND DISCUSSION

3.1 | Properties of coal samples

3.1.1 | Proximate and ultimate analyses

As shown in Table 1, both the ash and sulfur contents of PHSC are much lower than that of HSC, ie, 80% of the sulfur and 60% of the ash in HSC were removed by MCL treatment. This result proves that MCL method is an effective method to simultaneously eliminate the sulfur and ash contents in low-rank coal. In fact, MCL treatment transforms both the sulfur-containing contaminants and the metal minerals in coal into soluble inorganic sulfides, poly-sulfides, and other sulfides, and into soluble hydroxides or alkaline salts during the same processing. Then the soluble sulfur and inorganic compounds can be eliminated by water washing.²² In addition, the moisture

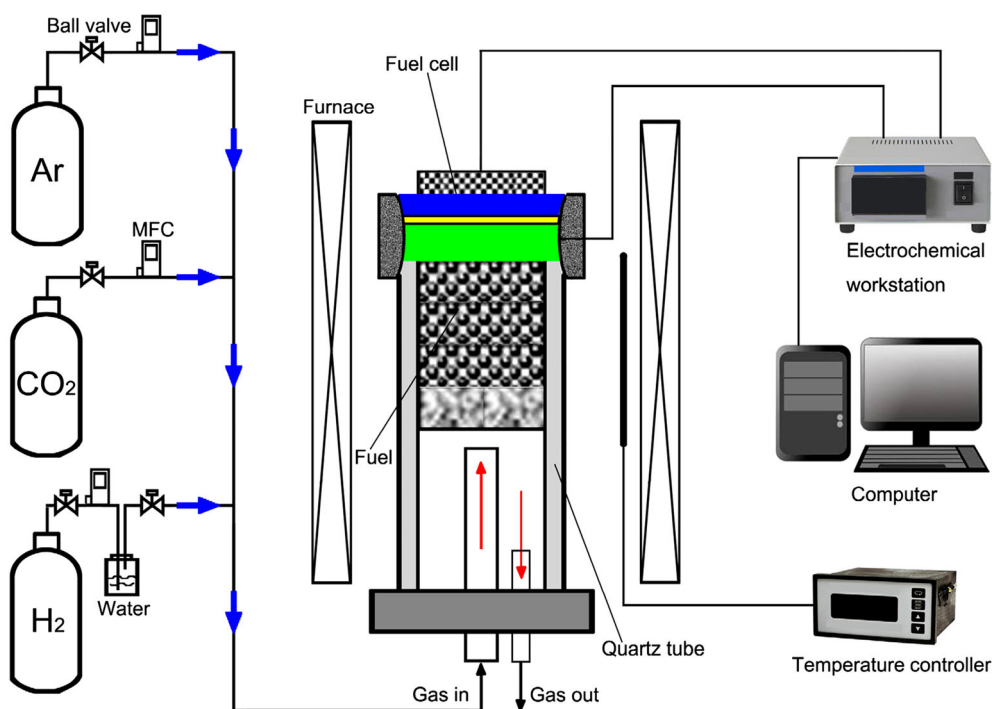


FIGURE 1 The schematic of fuel cell test setup [Colour figure can be viewed at wileyonlinelibrary.com]

TABLE 1 Proximate and ultimate analyses of HSC and PHSC

Sample	Proximate Analysis (wt%, air dry Basis)				Ultimate Analysis (wt%, air dry Basis)				
	M	A	V	FC	C	H	O	N	S _t
HSC	0.36	9.30	25.68	64.66	77.78	4.25	2.73	1.08	4.50
PHSC	1.13	1.86	18.35	78.66	76.25	4.01	2.95	1.16	1.80

Abbreviations: HSC, high-sulfur coal; PHSC, purified HSC. M, A, V, FC, and S_t denote moisture, ash, volatile, fixed carbon, and total sulfur, respectively.

content of PHSC is more than three times that of HSC, indicating that PHSC is prone to adsorb higher moisture amounts than HSC. This may happen due to the difference of microstructure between PHSC and HSC.

3.1.2 | Carbon crystalline structure and mineral phases

The XRD patterns of HSC and PHSC in Figure 2 exhibit 2 broad peaks within the diffraction ranges of 10° to 30° and 30° to 60°, known as the characterization of poorly crystalline carbon particles. Meanwhile, the XRD pattern of HSC shows various sharp diffraction peaks due to the existence of multiple mineral phases, which are assigned as kaolinite, quartz, pyrite, and so on.³² However, these mineral phase diffraction peaks almost disappear in the XRD pattern of PHSC, indicating that most of the inorganic minerals and sulfur impurities in HSC sample were removed by the MCL treatment. For understanding the chemical principle on the MCL process, the related chemical equations are shown as follows³³:

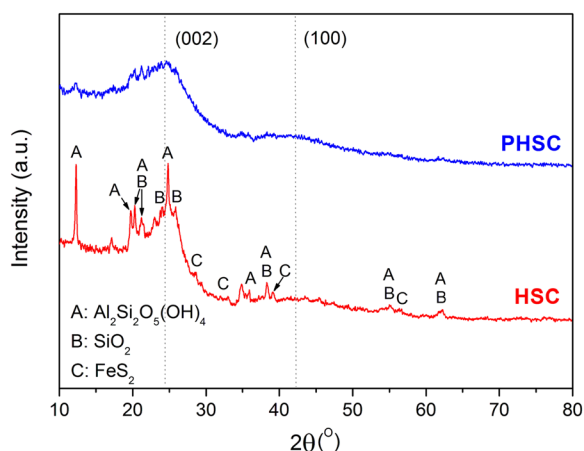
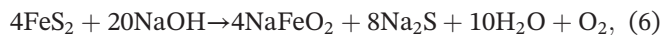


FIGURE 2 X-ray diffractometer spectra of high-sulfur coal and purified high-sulfur coal (PHSC) [Colour figure can be viewed at wileyonlinelibrary.com]

The changes in the (002) and (100) diffraction peaks of the coal samples reflect the evolution of carbon crystalline structures from HSC to PHSC. Table 2 lists the crystalline parameters, including the interplanar spacing (d_{002}), the average diameter (L_a), and the stacking height (L_c). Comparing HSC to PHSC, the values of d_{002} increase from 0.379 to 0.385 nm; however, both the L_c and L_a values decrease. These data indicate that PHSC has more loosely packed graphic structure and smaller microcrystal volume. The carbon microcrystal is geometrically assumed to be a cylinder, and its volume (V_{mc}) can be estimated by Equation 9.

$$V = \pi L_c \left(\frac{L_a}{2} \right)^2. \quad (9)$$

It is well known that the active sites of the Boudouard reaction in carbon materials are localized on the surface of the cylinder.^{1,29} A smaller volume of carbon microcrystals means a higher proportion of surface carbon atoms to the total carbon atoms within the microcrystals. Therefore, PHSC has a higher Boudouard reactivity than HSC.²⁹

3.1.3 | Chemical functional groups

FTIR was applied to identify the change of chemical functional groups when converting HSC to PHSC. To highlight this change, the whole wave number range is divided into 2 sections, ie, 400~2000 cm^{-1} (Figure 3A) and 2000~4000 cm^{-1} (Figure 3B). As shown in Figure 3A, the characteristic peaks of sulfur compounds located at ~472, ~540, ~1032, and 1260 cm^{-1} indicate the presence of relatively high sulfuric impurities, such as thiols, disulfides, sulfoxides, and sulfones in HSC. In addition, the mineral matter such as kaolinite (~914, 693 cm^{-1}), quartz (~802, 748 cm^{-1}), and carbonates (~1440, 872 cm^{-1}) are also observed for HSC.³⁴ However, these impurity peaks are significantly decreased even wiped out in the FTIR pattern of PHSC, revealing that most of the

TABLE 2 Carbon microcrystalline parameters of HSC and PHSC

Samples	d_{002} , nm	L_c , nm	L_a , nm	V_{mc} , nm^3
HSC	0.379	2.132	4.263	30.43
PHSC	0.385	1.421	3.423	13.07

Abbreviations: HSC, high-sulfur coal; PHSC, purified HSC.

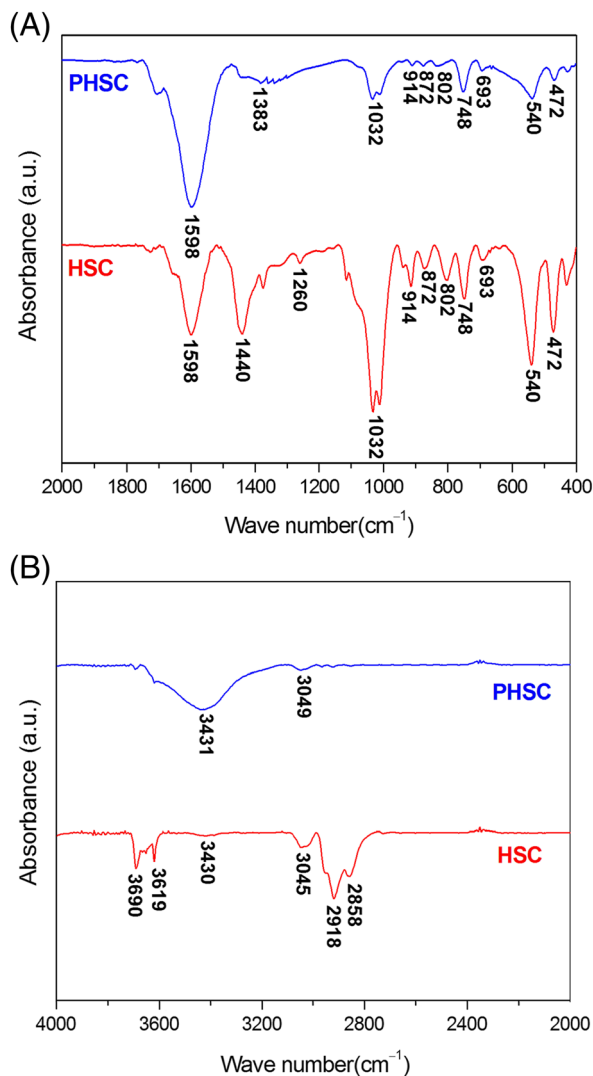


FIGURE 3 Fourier transform infrared spectroscopy spectra of high-sulfur coal (HSC) and purified HSC (PHSC) [Colour figure can be viewed at wileyonlinelibrary.com]

sulfuric impurities and mineral matter were removed by MLC treatment. The peaks at 1598 cm^{-1} in Figure 3A are assigned to the C=O (conjugated with C=C bonds) stretching vibrations of carbonyl groups.²⁹ The process of MLC treatment made the carbonyl group content in PHSC increase, which leads to the enhancement of the peak at 1598 cm^{-1} .

Compared with the FTIR spectra of HSC, the spectra of PHSC in Figure 3B has almost no Si/Al–OH stretching vibration peaks ($3619\text{--}3690\text{ cm}^{-1}$), indicating the removal of mineral matter such as kaolinite. In addition, the aromatic C–H stretching vibrations ($2808\text{--}3045\text{ cm}^{-1}$) in the spectra of PHSC are highly weakened, indicating that the aromatic structures were partially destroyed. However, the characteristic self-associated O–H stretch vibrations in hydroxyl groups ($\sim 3431\text{ cm}^{-1}$) are greatly strengthen for PHSC, indicating that through the MCL

treatment, the hydroxyl groups in the surface of PHSC were highly increased.^{29,35,36} In short, the increase of oxygen-containing functional groups and the reformation of aromatic structures may result in the improvement of gasification reactivity of PHSC.

3.1.4 | Textural structure and morphology

The textural properties of carbon fuels also closely correlate with their chemical and electrochemical reactivity. The specific surface areas, pore volumes, and average pore sizes of HSC and PHSC were determined by N_2 adsorption experiments, a powerful method to characterize textural property of carbon materials. As shown in Table 3, the BET surface area and total pore volume of PHSC are increased to 3.8 times and 2.5 times that of HSC, respectively. Meanwhile, the average pore size of PHSC decreased, indicating that new pores were produced due to the removal of mineral matter from HSC. The results indicate that PHSC should have more reactive sites in favor of its Boudouard gasification.

Figure 4 shows the morphologies of HSC and PHSC under SEM. There is a clear variation in the morphology from HSC to PHSC. The surface of HSC particles (Figure 4A) is relatively rough, with sharp edges, and almost no pores there. For PHSC particles shown in Figure 4B, a mesoporous structure appears on the surface. Meanwhile, the surface of PHSC becomes smoother and the shape becomes rounder. The porous structure of PHSC may stem from the removal of sulfur and mineral matter by MCL treatment. The appearance of porous structure of PHSC is consistent well with its higher specific surface areas in N_2 adsorption experiments.

3.2 | Thermal stability and oxidation reactivity of coal samples

TG analysis is an effective method to investigate thermal stability and oxidation reactivity of carbon materials.^{24,25} DTG analysis can precisely provide the information of the initial and final reaction temperatures, and the

TABLE 3 Specific surface areas and pore parameters of the HSC and PHSC

	HSC	PHSC	Ratio of PHSC to HSC
BET surface area	3.60	13.71	3.8
Total pore volume, $\text{cm}^3\text{ g}^{-1}$	0.0102	0.0259	2.5
Average pore size, nm	11.35	7.55	0.7

Abbreviations: BET, Brunauer-Emmett-Teller; HSC, high-sulfur coal; PHSC, purified high-sulfur coal.

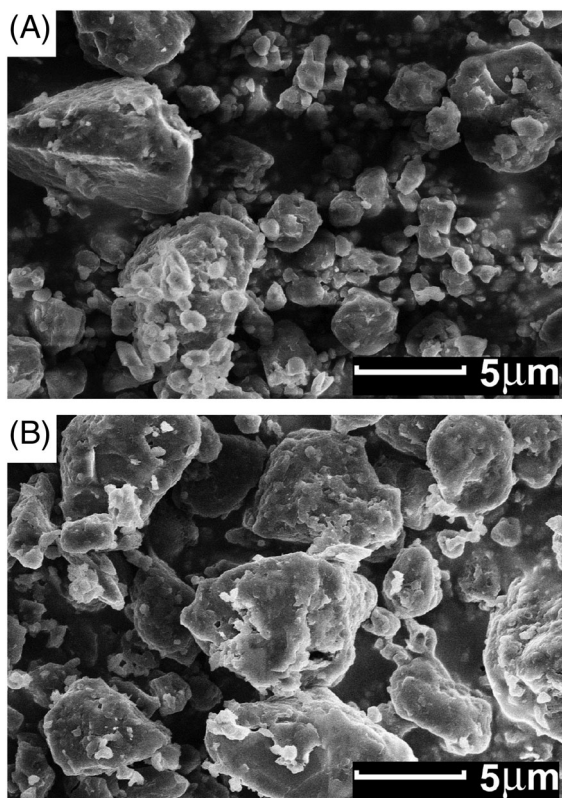


FIGURE 4 Scanning electron microscope images of A, high-sulfur coal and B, purified high-sulfur coal

temperature at which the weight loss rate reaches its maximum value. Combining the TG and DTG profiles shown in Figure 5A,B, the features of thermal stability and oxidation reactivity of HSC and PHSC can be summarized as follows. Under Ar atmosphere, HSC and PHSC have a relatively low DTG peak centered at approximately 480°C and 80°C, respectively, indicating the release of volatile matter from HSC and the loss of moisture of PHSC. From 120 to 1000°C, the weight decrease of PHSC is almost linear. As for HSC, the weight decreasing tendency is also nearly linear, with the exception of the range from 390°C to 540°C.

Under air atmosphere, the whole temperature range can be divided into 3 sections where distinct thermochemical processes occur: (1) the moisture loss section from ambient temperature to 140°C, (2) the thermal decomposition section from 140°C to 360°C, and (3) the char combustion section from 360°C to 1000°C.³⁷ In the moisture loss section, only PHSC has a peak centered at 75°C. The smooth platform for HSC suggests that the moisture content in HSC is too little to be detected. This distinct capability for adsorbing ambient moisture between HSC and PHSC should stem from the different specific surface areas. In fact, the specific surface area of PHSC is 3.8 times that of HSC (according to the BET results revealed in Table 2). In the thermal decomposition section, only

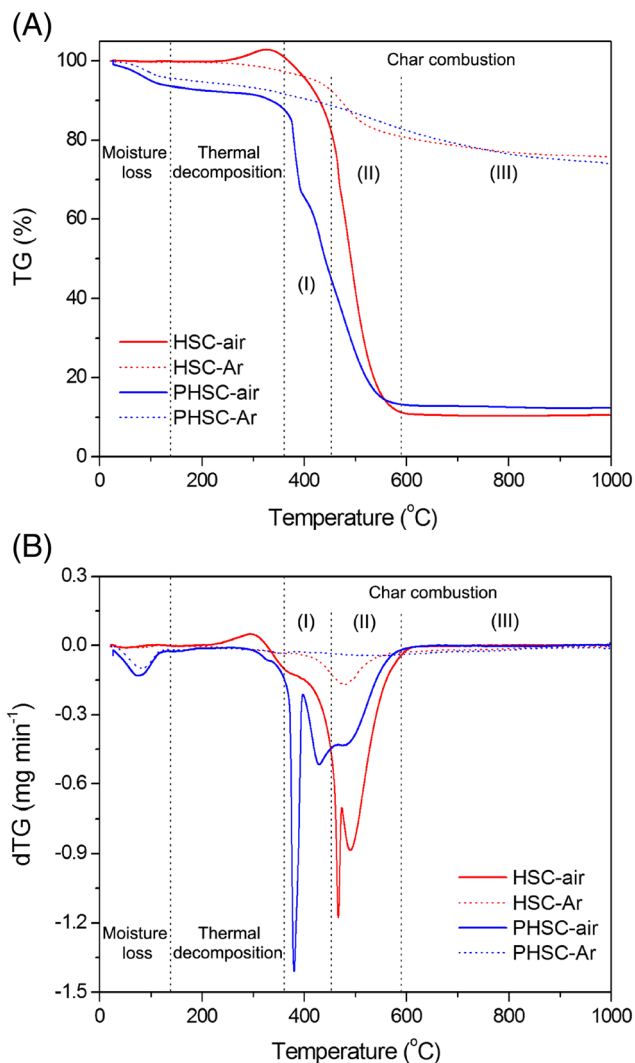


FIGURE 5 A, Thermogravimetric (TG) mass loss curves and B, differential thermogravimetric (DTG) curves of the coal samples in air (solid line) and in Ar atmosphere (dashed line) [Colour figure can be viewed at wileyonlinelibrary.com]

HSC has a surprising positive peak centered around 295°C, indicating that some constituents in HSC have reacted with the oxygen in the atmospheric air forming additional oxides. The gentle decline line of PHSC reflects the increase of volatile matter from the conversion of HSC into PHSC. The char combustion section is the most complex one, which can be divided into 3 subsections for clearer analysis. It is important to note that there is a crossover point of the lines at 452°C. In fact, it is the critical point to distinguish the thermochemical behavior of the 2 samples. The first subsection is in the range from 360°C to 452°C, where PHSC has a faster oxidation rate than that of HSC, with the fastest rate at 380°C. However, the situation totally reverses for the second sub-section in the range from 452 to 590°C, where HSC has a faster oxidation rate than that of PHSC, with the fastest rate at 466°C. In the third subsection, the lines of HSC and PHSC

merge together into one platform until the end of the experiment.

In short, the result of the char combustion section reveals that the oxidation reactivity of PHSC is superior to that of HSC, that is, nearly two-thirds of the fixed carbon of PHSC are gasified at the lower temperature range. However, in the case of HSC, it is just less than one quarter.

3.3 | Electrochemical performance of fuel cells fed with HSC or PHSC

The cross-sectional image in Figure 6A shows that the YSZ electrolyte layer is quite dense, only with few closed pores without negative influence on the gas tightness of the cell. Both the porous anode (Figure 6B) and cathode (Figure 6A) layers have relatively uniform microstructures and attach closely to the electrolyte substrate. The anode layer has a thickness of approximately 0.47 mm with the porosity of approximately 29% (Archimedes method). The microstructure of the fuel cell guarantees gas tightness and reliability.

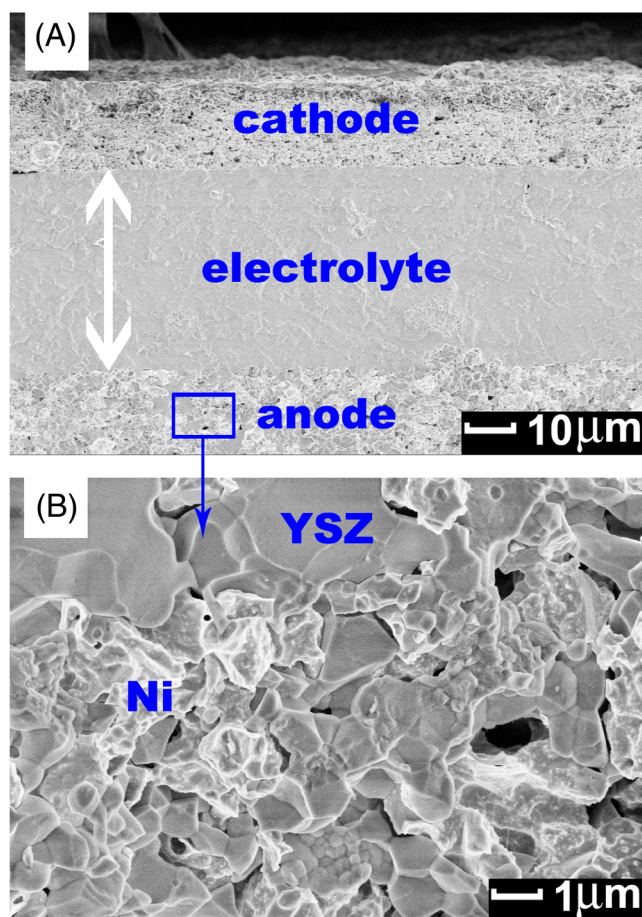


FIGURE 6 Scanning electron microscope images of the A, cross section and B, anode surface of the fuel cell [Colour figure can be viewed at wileyonlinelibrary.com]

Figure 7 presents the EIS of cells fed with HSC and PHSC at temperatures from 800°C to 900°C. On one hand, an identical feature can be seen in Figure 7A,B, that is, the ohmic resistances (R_o) of the cells fed with HSC or PHSC increase slightly but the overall polarization resistances (R_p) increase significantly with the decrease of operational temperature. The increase of R_o is mainly attributed to the increase of electrolyte resistance. In general, the ohmic resistance from the electrolyte is far greater than those from the current collectors and related metal conducting wires, and from the interface resistances between the electrolyte and the current collectors with the cathode or anode. With decreasing temperature, the electrolyte resistance normally increases more noticeably than those of the interface resistances. The ohmic resistance from the metal current collectors and related metal conducting wires usually decreases with decreasing temperature. The polarization resistance (R_p) is influenced by both anode and cathode polarization impedances that increase along with a decreasing temperature. Given the fact that the anode polarization impedance includes both activation and mass transport resistances and since both the cathode polarization and the anode activation resistances are almost constant (for the cells fed with PHSC and HSC), then, the anode mass transport resistance should be the main reason behind this significant difference of R_p . Another important aspect to be noted is the fact that the R_p values of cells fed with HSC were always greater than those of cells fed with PHSC at corresponding temperatures.

To clearly identify the anode mass transport resistance differences between the cells fed with HSC and PHSC, the EIS curves of resistance versus frequency are given in Figure 7C,D. Generally, high frequency (HF > 10 kHz) response arises from the electrolyte resistance, and the medium frequency (MF, 100-10 kHz) responses are related to the impedance of the electron-transfer and ion-transfer processes occurring at the current collector/electrode and electrode/electrolyte interfaces, respectively.³⁸⁻⁴⁰ The response at the low frequency (LF, 0.1-100 Hz) normally arises from the concentration polarization in the porous anode, which is related to the fuel gas diffusion rate and the gas concentration in the anode chamber.⁴⁰

As shown in Figure 7C,D, regardless of the chosen fuel or operating temperature, there is almost no difference between the EIS lines at the frequencies above 10^2 Hz. On the contrary, at the range of frequency $<10^2$ Hz, significant differences in the EIS lines appear. With decreasing temperature, the resistances increase substantially both for HSC and PHSC. However, at each operating temperature, the values of R_p for HSC are almost 2 times that for PHSC at the correspondence frequency. Therefore, the

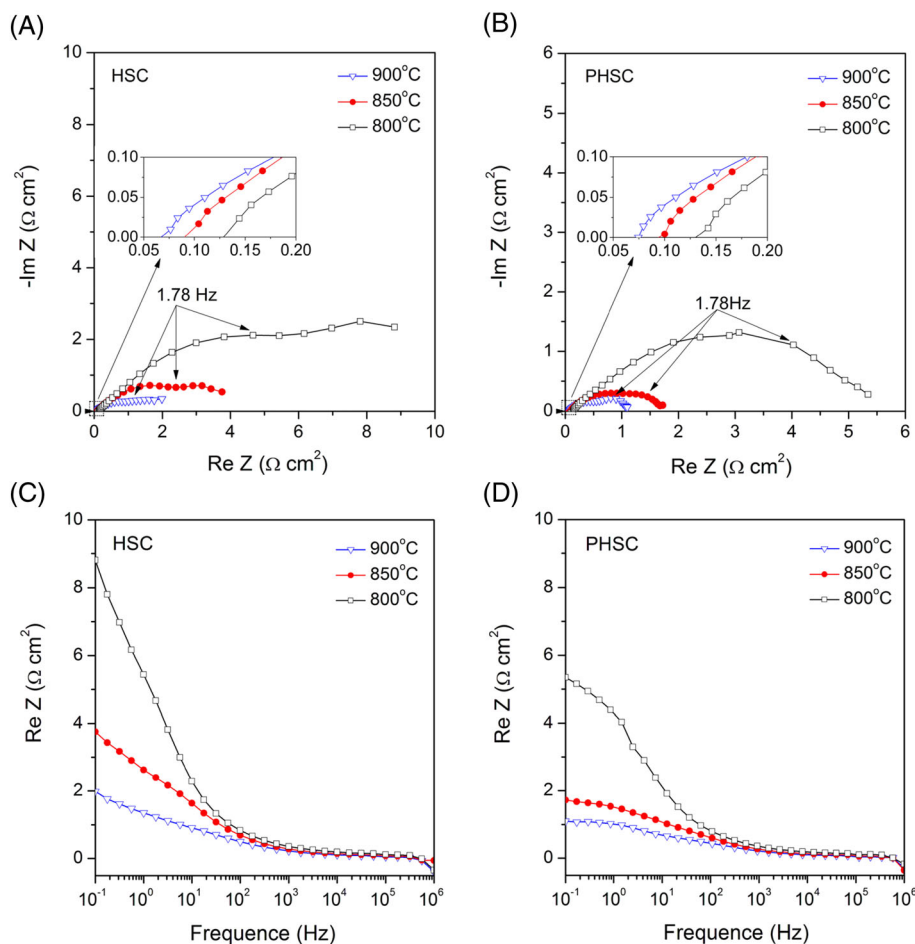


FIGURE 7 Electrochemical impedance spectra of the cells fuelled with A and C, HSC and B and D, PHSC at various temperatures. The insets in A and B are the magnified parts of the spectra to show the R_o clarity [Colour figure can be viewed at wileyonlinelibrary.com]

marked difference of R_p in the low frequency range ($<10^2$ Hz) definitely indicates that the anode mass transport resistances dominate the significant difference of R_p between HSC and PHSC.

The resistance of anode mass transport of DC-SOFCs is closely related to the CO diffusion rate and the CO quantity produced by the Boudouard gasification of fuels in the anode. The change of operating temperature not only impacts the cell itself, but also on the Boudouard reactivity of fuels. The later effect results in the R_p difference in low-frequency zone. It has been confirmed that the concentration polarization in the anode is strongly correlated with the partial pressure of fuel gases at the anode reaction sites. The smaller mass transport resistances in Figure 7D stem from a greater supply of CO produced by the Boudouard gasification of PHSC to the anode. This is very consistent with the results of TG and DTG (Figure 5), that is, PHSC has higher gasification reactivity than HSC, thus can produce more CO in the anode region and result in smaller mass transport resistances. The EIS analyses lay a foundation to understand the other electrochemical performance shown in Figure 8.

Figure 8A,B shows the output performance of the cells fed with HSC and PHSC in temperatures from 800°C to 900°C. It is important to note that the PPD of cells fed with PHSC is always higher than that of cells fed with HSC at corresponding temperatures. For example, at 900°C, the PPD value in using PHSC fuel achieves 221 mW cm^{-2} , which is almost twice as much as the one with HSC (115 mW cm^{-2}). It is important to intensify that this PPD value using HSC was already a relatively remarkable performance considering the reported results of coal fuel cells up to now. With increasing temperature, the PPDs of the cells fed both with HSC and PHSC increase dramatically. The reasons can be found in the results of Figure 7. The R_o and R_p of the cells both decrease with increasing temperature. The improvement of Boudouard gasification rate of fuels with increasing temperature leads to more sufficient supply of CO to the anode active sites, which favors the decrease of concentration polarization and the increase of output performance.^{18,41-45}

Figure 8C shows that the open circuit voltage (OCV) of cells fed with PHSC is higher than that of cells using HSC fuel at corresponding temperature. The theoretical

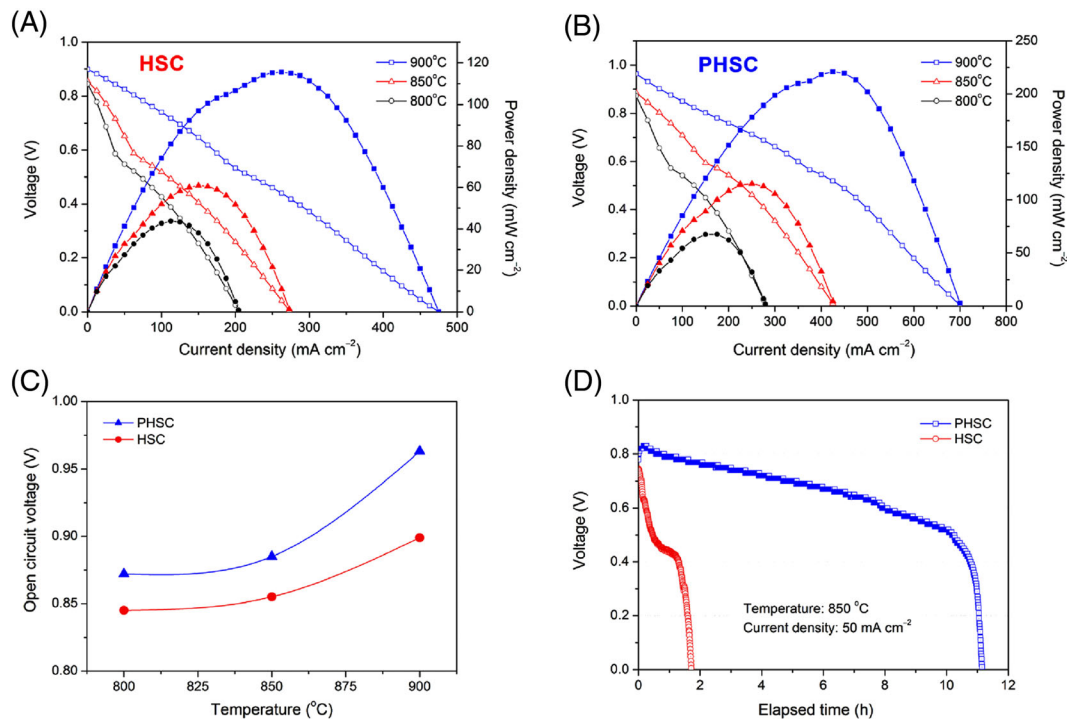


FIGURE 8 I-V and I-P curves for the cells fuelled with A, high-sulfur coal (HSC) and B, purified HSC (PHSC) at various temperatures. C, Open circuit voltage comparison at various temperatures. D, Stability test of the cells fuelled with HSC and PHSC at 50 mA cm⁻² under 850°C [Colour figure can be viewed at wileyonlinelibrary.com]

OCV of DC-SOFCs can be calculated according to the Nernst equation:

$$E = E^0 + \frac{RT}{4F} \ln \left[P_{O_2}^c \cdot \left(\frac{P_{CO}^a}{P_{CO_2}^a} \right)^2 \right], \quad (10)$$

where E^0 is the standard electro-motivated potential and $P_{O_2}^c$, P_{CO}^a , and $P_{CO_2}^a$ denote the partial pressures of O_2 at the cathode side and CO and CO_2 in the anode chamber, respectively. According to Equation 10, PHSC with higher Boudouard reactivity can maintain higher ratio of $P_{CO}^a/P_{CO_2}^a$ in the anode chamber, thus leads to higher OCV values than HSC.

Figure 8D shows the stability test of cells fed with HSC and PHSC at a constant current density of 50 mA cm⁻² at 850°C. The terminal voltage of the cell fed with HSC decreases significantly in the initial period and maintains a short time at low potential of 0.4 V, then quickly drops to zero. On the contrary, the voltage of the cell fed with PHSC maintains a quite long term nearly 11 hours at a high enough level (above 0.5 V) with a gently degradation slope. The stability of the cells fed with HSC is very poor when compared with that of PHSC, which is definitely due to the contaminants in HSC, such as S, Si, and Al compounds. It is well known that sulfur-containing impurities have severe poisoning effect on nickel-based catalysts, and the Si and Al oxides tend to suppress the Boudouard gasification.⁴⁶⁻⁴⁸ The combination of sulfur

deactivated nickel anode with less supply of CO gas from the inhibited Boudouard gasification of HSC leads to a considerable degradation in the cell performance. In the case of PHSC, the elimination of most of the sulfur and mineral matter by MCL method reduces the negative effects to a controllable extent, which do help to improve the electrochemical performance and maintain a reasonable durability.

The availability of coal-derived carbon is an important index for evaluating its applicability in DC-SOFCs. The availabilities were tested at a constant current density of 50 mA cm⁻² at 800°C according to the following equation:

$$\eta_{\text{carbon}} = \frac{C_{\text{elec}}}{C_{\text{ld}}} \times 100\%, \quad (11)$$

where C_{elec} and C_{ld} represent the masses of carbon converted electrochemically and carbon loaded in the anode chamber, respectively. As shown in Table 4, the availability of the cell fed with PHSC is 40%, approximately 6.4 times that of HSC (6.25%), indicating that the PHSC is a promising candidate for using as a fuel for DC-SOFCs. This result is consistent with the physicochemical properties and electrochemical performance of PHSC aforementioned. Here, more than half of the fuels were not used via electrochemical reaction. This may be attributed to carbon fuel losses caused by secondary gases formation via thermal decomposition and the reverse Boudouard

TABLE 4 Information of availability of SOFCs fuelled with HSC and PHSC

Fuels	Discharge Time, h	Electric Quantity, C	Carbon Converted, g	Carbon Loaded, g	Availability, %
HSC	1.72	149	0.001	0.16	6.25
PHSC	11.15	964	0.06	0.15	40

Abbreviations: HSC, high-sulfur coal; PHSC, purified HSC; SOFCs, solid oxide fuel cells.

reaction, which is in reasonable agreement with the previous work.⁴⁸ Further work is needed to improve the availability of coal-derived carbon fuels.

3.4 | Postmortem analysis

Figure 9A,C reveals the corresponding SEM images of the surface of nickel cermet anodes after performing the stability test of the cells fuelled with HSC and PHSC. Figure 9B,D are the corresponding EDX spectra, respectively. From Figure 9A,C, it can be found that the surface of nickel cermet anode seems to be contaminated to more severe extent in the case of using HSC fuel. Figure 9B,D provide more detailed information. To support this statement, the strongest and stronger peaks respond to the elements of zirconium (Zr), yttrium (Y), oxygen (O), and nickel (Ni), which reflect the chemical composition of the anode materials. In addition, the elements of carbon (C) and sulfur (S) also appear in the spectra, indicating that the sulfur poisoning and carbon deposition occurred on the anode surfaces of cells fuelled with HSC or with PHSC. However, there is a big gap between HSC and

PHSC in terms of the accumulation quantity and deposition rate of carbon and sulfur. The weight percent quantities of carbon and sulfur elements in the case of using HSC fuel (Figure 9B) are approximately 2 and 3 times those of using PHSC fuel (Figure 9D), respectively. In the point of view of kinetics, the deposition rate of carbon and sulfur also displays a great difference between HSC and PHSC. As shown in Figure 9B, the accumulation quantities of sulfur and carbon on the nickel cermet anode reach up to 0.44 and 21.81 wt%, respectively, within the cell lifetime of 1.72 hours. These values mean deposition rates of 0.26 wt\% h^{-1} and $12.68 \text{ wt\% h}^{-1}$ (regarding sulfur and carbon) for cells fuelled with HSC. As for PHSC (Figure 9D), in the cell lifetime of 11.15 hours, quantities of these elements on the anode are only 0.15 wt% (of sulfur) and 11.3 wt% (of carbon), corresponding to the deposition rates of 0.013 and 1.01 wt\% h^{-1} (which represent approximately 5% and 8% of the values obtained with HSC).

In summary, the result confirms that compared to HSC, PHSC, when using as a fuel, can greatly improve the electrochemical performance and the durability of

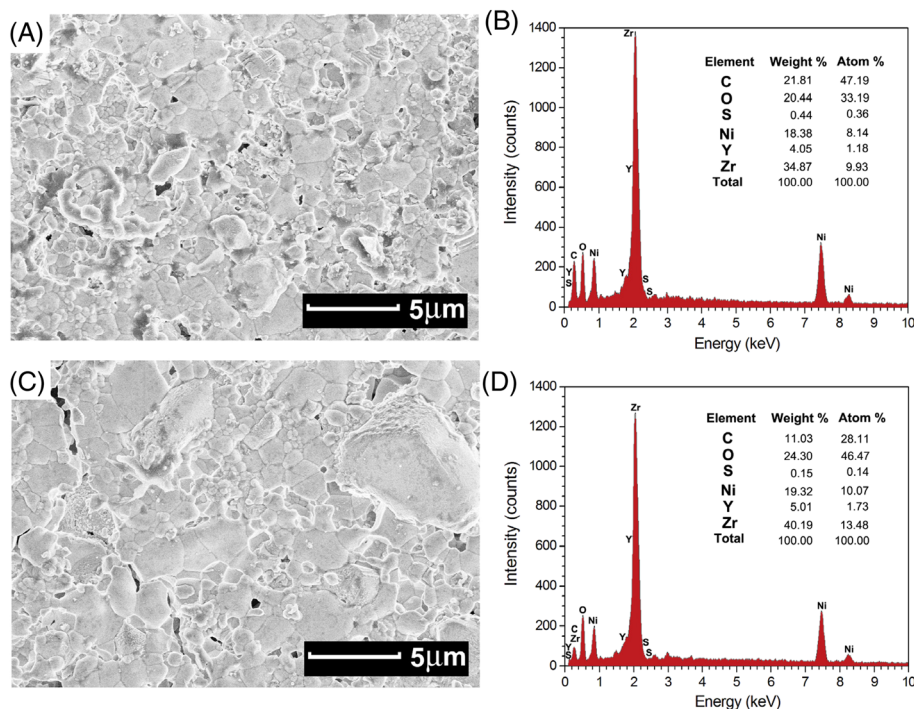


FIGURE 9 Scanning electron microscope images and energy dispersive X-ray analyzer spectra of anode surfaces after test. A and B, high-sulfur coal fuel. C and D, purified high-sulfur coal fuel [Colour figure can be viewed at wileyonlinelibrary.com]

the fuel cell due to less sulfur poisoning and carbon deposits on the nickel cermet anode. However, based on the results shown in this work, we think that much effort should be focused on the following issues for further improving the operation stability of DC-SOFCs using PHSC as fuel for practical application: (1) the development of new anode materials with high sulfur tolerance and coking resistance capabilities; (2) the materials and methods for in situ capture and sequestration of sulfur-containing gaseous compounds in the anode chamber to solve the residual sulfur problem; and (3) the continuous feed of solid carbon fuels to the anode for long-term operation of cells.

4 | CONCLUSIONS

The compatibility of an HSC and the purified contrast with a nickel-based anode SOFC is examined in this work. Desulfurization of the pristine coal by MCL method reaches the removal ratio of 80%. Property analyses of coal samples indicate that the purified coal has a more advantageous structure and higher Boudouard reactivity suitable as a fuel for fuel cells. The fuel cells fed with the purified coal have significantly improved performance: The PPD achieves 221 mW cm^{-2} at 900°C and the durability of 11.2 hours under 50 mA cm^{-2} is accomplished at 850°C with a fuel availability of 40%. The fuel-based investigation reveals that the purified coal is a promising fuel for DC-SOFCs. Further developments both on more effective purification methods for low-rank coal and on the anode materials with higher sulfur tolerance would be required to achieve a high fuel compatibility and long-term sustained performance.^{49,50}

ACKNOWLEDGEMENTS

This work was supported by the Shanxi Key Technologies R&D Program (20150313003-3), the Shanxi Natural Science Foundation (201601D102014), the Shanxi Coal-bed Methane Joint Foundation (2015012016), and the Shanxi Program for the Sci-tech Activities of Returnee Scholars (2014). The authors acknowledge the Australian Research Council for supporting the project under contracts DP150104365 and DP160104835. Wenting An and Yong Jiao (201608140134) would like to thank the Curtin University and the China Scholarship Council for offering a visiting scholarship, respectively.

ORCID

Yong Jiao  <http://orcid.org/0000-0002-4947-2303>

Wenting An  <http://orcid.org/0000-0002-5589-2988>

REFERENCES

- Jiang C, Ma J, Corre G, Jain SL, Irvine JTS. Challenges in developing direct carbon fuel cells. *Chem Soc Rev*. 2017;46(10):2889-2912.
- Cao T, Huang K, Shi Y, Cai N. Recent advances in high-temperature carbon-air fuel cells. *Energy Environ Sci*. 2017;10(2):460-490.
- Gür TM. Progress in carbon fuel cells for clean coal technology pipeline. *Int J Energy Res*. 2016;40(1):13-29.
- Zhou W, Jiao Y, Li SD, Shao Z. Progress on anodes for carbon-fueled solid oxide fuel cells: a mini review. *ChemElectroChem*. 2015;3(2):193-203.
- Cao D, Sun Y, Wang G. Direct carbon fuel cell: fundamentals and recent developments. *J Power Sources*. 2007;167(2):250-257.
- Gür TM. Critical review of carbon conversion in carbon fuel cells. *Chem Rev*. 2013;113(8):6179-6206.
- Giddey S, Badwal SPS, Kulkarni A, Munnings C. A comprehensive review of direct carbon fuel cell technology. *Prog Energy Combust Sci*. 2012;38(3):360-399.
- Wang W, Su C, Wu Y, Ran R, Shao Z. Progress in solid oxide fuel cells with nickel-based anodes operating on methane and related fuels. *Chem Rev*. 2013;113(10):8104-8151.
- Ni M, Leung MKH, Leung DYC. Ammonia-fed solid oxide fuel cells for power generation—a review. *Int J Energy Res*. 2009;33(11):943-959.
- Xu H, Chen B, Zhang H, Sun Q, Yang G, Ni M. Modeling of direct carbon solid oxide fuel cells with H_2O and CO_2 as gasification agents. *Int J Hydrogen Energy*. 2017;42(23):15641-15651.
- Xu H, Chen B, Liu J, Ni M. Modeling of direct carbon solid oxide fuel cell for CO and electricity cogeneration. *Appl Energy*. 2016;178:353-362.
- Jiang C, Ma J, Bonaccorso AD, Irvine JTS. Demonstration of high power, direct conversion of waste derived carbon in a hybrid direct carbon fuel cell. *Energy Environ Sci*. 2012;5(5):6973-6980.
- Xu X, Zhou W, Liang F, Zhu Z. A comparative study of different carbon fuels in an electrolyte-supported hybrid direct carbon fuel cell. *Appl Energy*. 2013;108:402-409.
- Nakagawa N, Ishida M. Performance of an internal direct-oxidation carbon fuel cell and its evaluation by graphic exergy analysis. *Ind Eng Chem Res*. 1988;27(7):1181-1185.
- Gür TM, Huggins RA. Direct electrochemical conversion of carbon to electrical energy in a high temperature fuel cell. *J Electrochem Soc*. 1992;139(10):L95-L97.
- Wu Y, Su C, Zhang C, Ran R, Zhao Z. A new carbon fuel cell with high power output by integrating with in situ catalytic reverse Boudouard reaction. *Electrochem Commun*. 2009;11(6):1265-1268.
- Tang Y, Liu J. Effect of anode and Boudouard reaction catalysts on the performance of direct carbon solid oxide fuel cells. *Int J Hydrogen Energy*. 2010;35(20):11188-11193.
- Li C, Shi Y, Cai N. Performance improvement of direct carbon fuel cell by introducing catalytic gasification process. *J Power Sources*. 2010;195(15):4660-4666.
- Liu R, Zhao C, Li J, et al. A novel direct carbon fuel cell by approach of tubular solid oxide fuel cells. *J Power Sources*. 2010;195(2):480-482.

20. Bao JE, Krishnan GN, Jayaweera P, Perez-Mariano J, Sanjurjo A. Effect of various coal contaminants on the performance of solid oxide fuel cells: part I. Accelerated testing. *J Power Sources*. 2009;193(2):607-616.
21. Gür TM, Homel M, Virkar AV. High performance solid oxide fuel cell operating on dry gasified coal. *J Power Sources*. 2010;195(4):1085-1090.
22. Wahab A, Nawaz S, Shahzad K, et al. Desulfurization and demineralization of lakhra coal by molten caustic leaching. *Energy Sources, Part A*. 2015;37(11):1219-1223.
23. Li X, Zhu Z, De Marco R, Bradley J, Dicks A. Evaluation of raw coals as fuels for direct carbon fuel cells. *J Power Sources*. 2010;195(13):4051-4058.
24. Rady AC, Giddey S, Kulkarni A, Badwal SPS, Bhattacharya S, Ladewig BP. Direct carbon fuel cell operation on brown coal. *Appl Energy*. 2014;120:56-64.
25. Ju HK, Eom J, Lee JK, et al. Durable power performance of a direct ash-free coal fuel cell. *Electrochim Acta*. 2014;115:511-517.
26. Jewulski J, Skrzypkiewicz M, Struzik M, Lubarska-Radziejewska I. Lignite as a fuel for direct carbon fuel cell system. *Int J Hydrogen Energy*. 2014;39(36):21778-21785.
27. Dudek M. On the utilization of coal samples in direct carbon solid oxide fuel cell technology. *Solid State Ion*. 2015;271:121-127.
28. Jiao Y, Tian W, Chen H, et al. *In situ* catalyzed Boudouard reaction of coal char for solid oxide-based carbon fuel cells with improved performance. *Appl Energy*. 2015;141:200-208.
29. Jiao Y, Zhao J, An W, et al. Structurally modified coal char as a fuel for solid oxide-based carbon fuel cells with improved performance. *J Power Sources*. 2015;288:106-114.
30. Dudek M, Skrzypkiewicz M, Moskała N, Grzywacz P, Sitarz M, Lubarska-Radziejewska I. The impact of physicochemical properties of coal on direct carbon solid oxide fuel cell. *Int J Hydrogen Energy*. 2016;41(41):18872-18883.
31. Shao Z, Zhang C, Wang W, et al. Electric power and synthesis gas co-generation from methane with zero waste gas emission. *Angew Chem Int Ed*. 2011;50(8):1792-1797.
32. Li X, Zhu Z, Chen J, et al. Surface modification of carbon fuels for direct carbon fuel cells. *J Power Sources*. 2009;186:1-9.
33. Duz MZ, Saydut A, Erdogan S, Hamamci C. Removal of sulfur and ash from coal using molten caustic leaching, a case study from Hazro fields, Turkey. *Energy Explor Exploit*. 2009;27(6):391-400.
34. He X, Zhang X, Jiao Y, et al. Complementary analyses of infrared transmission and diffuse reflection spectra of macerals in low-rank coal and application in triboelectrostatic enrichment of active maceral. *Fuel*. 2017;192:93-101.
35. Song Y, Jiang B, Mathews JP, Yan G, Li F. Structural transformations and hydrocarbon generation of low-rank coal (vitrinite) during slow heating pyrolysis. *Fuel Process Technol*. 2017;167:535-544.
36. Manoj B, Kunjomana AG. Chemical leaching of an Indian bituminous coal and characterization of the products by vibrational spectroscopic techniques. *Int J Miner Metall Mater*. 2012;19(4):279-283.
37. Park JM, Keel S, Ji Y, Yun JH, Lee SS. Thermogravimetric study for the co-combustion of coal and dried sewage sludge. *Korean J Chem Eng*. 2017;34(8):2204-2210.
38. Jiao Y, Zhang L, An W, et al. Controlled deposition and utilization of carbon on Ni-YSZ anodes of SOFCs operating on dry methane. *Energy*. 2016;113:432-443.
39. Adler SB. Factors governing oxygen reduction in solid oxide fuel cell cathodes. *Chem Rev*. 2004;104(10):4791-4844.
40. Kennouche D, Chen-Wiegart YCK, Riscoe C, Wang J, Barnett SA. Combined electrochemical and X-ray tomography study of the high temperature evolution of Nickel-Yttria Stabilized Zirconia solid oxide fuel cell anodes. *J Power Sources*. 2016;307:604-612.
41. Zhong Y, Su C, Cai R, Tadé MO, Shao Z. Process investigation of a solid carbon-fueled solid oxide fuel cell integrated with a CO₂-permeating membrane and a sintering-resistant reverse Boudouard reaction catalyst. *Energy and Fuels*. 2016;30(3):1841-1848.
42. Xie Y, Tang Y, Liu J. A verification of the reaction mechanism of direct carbon solid oxide fuel cells. *J Solid State Electrochem*. 2013;17(1):121-127.
43. Cai W, Liu J, Yu F, et al. A high performance direct carbon solid oxide fuel cell fueled by Ca-loaded activated carbon. *Int J Hydrogen Energy*. 2017;42(33):21167-21176.
44. Yu X, Shi Y, Wang H, Shi Y, Cai N, Ghoniem AF. Using potassium catalytic gasification to improve the performance of solid oxide direct carbon fuel cells: experimental characterization and elementary reaction modeling. *J Power Sources*. 2014;252:130-137.
45. Yu X, Shi Y, Wang H, et al. Experimental characterization and elementary reaction modeling of solid oxide electrolyte direct carbon fuel cell. *J Power Sources*. 2013;243:159-171.
46. Matsuzaki Y, Yasuda I. The poisoning effect of sulfur-containing impurity gas on a SOFC anode: part I. Dependence on temperature, time, and impurity concentration. *Solid State Ion*. 2000;132(3):261-269.
47. Tulloch J, Allen J, Wibberley L, Donne S. Influence of selected coal contaminants on graphitic carbon electrooxidation for application to the direct carbon fuel cell. *J Power Sources*. 2014;260:140-149.
48. Nürnberger S, Buřar R, Desclaux P, Franke B, Rzepka M, Stimming U. Direct carbon conversion in a SOFC-system with a non-porous anode. *Energy Environ Sci*. 2010;3(1):150-153.
49. Xu X, Zhou W, Liang F, Zhu Z. Optimization of a direct carbon fuel cell for operation below 700°C. *Int J Hydrogen Energy*. 2013;38(13):5367-5374.
50. Kim H, Hong J, Yoon KJ, et al. High-performance and robust operation of anode supported solid oxide fuel cells in mixed-gas atmosphere. *Int J Energy Res*. 2016;40(6):726-732.

How to cite this article: Jiao Y, Xue X, An W, et al. Purified high-sulfur coal as a fuel for direct carbon solid oxide fuel cells. *Int J Energy Res*. 2019;43:2501–2513. <https://doi.org/10.1002/er.4004>